INELASTIC ELECTRON SCATTERING

C. Colliex, C. Mory and P. Trebbia
Laboratoire de Physique des Solides associé au CNRS
Bâtiment 510, Université Paris-Sud
91405 Orsay France

1. Elastic and inelastic processes.

Various types of collision processes between complex particles are generally classified, see for instance Messiah[1], as follows :

- elastic collisions of type $A + B \rightarrow A + B$ with only a change in relative momentum between the initial and final states which correspond to the same channel,
- inelastic collisions of type $A + B \rightarrow A^* + B^*$ which involve a change of internal quantum state and consequently different input and output channels but the same interaction potential in these channels,
- rearrangement collisions of type $A + B \rightarrow C + D$ which involve exchange of particles between the two partners of the collision.

In the specific case of scattering of high energy electrons by solids, exchange effects are neglected and one only considers elastic and inelastic collisions. In the transmission electron microscope the beam of quasimonochromatic electrons of primary energy E_o interacts with the specimen so that most of the outgoing electrons have suffered changes in direction and in energy. From the experimental point of view, the term inelastic process with an energy loss ΔE is used when the measured change in energy (ΔE) is larger than the smallest detectable one (δE) with the spectrometer which is used. In most cases this lower limit is set by the width of the primary beam at about 1 eV.

A complete knowledge of the distribution in momentum ($\vec{q}$) and energy (ΔE) of the transmitted electrons is therefore necessary to characterize the scattering properties of the target and consequently to reveal its static and dynamical behaviour . Rather few measurements of this type have been achieved ; this is mainly due to the large dynamic range which is necessary to compare the intensities at q and $\Delta E = 0$ and at large q and ΔE : it easily reaches ratios of the order of 10^6 to 10^8 : 1. To obtain satisfactory data over a large number of experimental points, computer aided systems combining an automatic recording of spectra such as $I_{\Delta E}(q)$ and (or) $I_q(\Delta E)$ and electron counting capabilities are required.

The results must be displayed as a three-dimensional chart $I(\Delta E,q)$ for an amorphous or polycrystalline specimen with a cylindrically symmetric angular distribution of scattered electrons. The first systematic work of this type is due to Batson (2) for the valence electron excitation spectrum in aluminium. His results are displayed as intensity contour maps as a function of ΔE in eV and q in $\mathring{A}^{-1}$, similar to the example shown in figure 1. We are now extending such measurements to other elements (carbon, gold ...) ; some partial data are shown in figure 2, as a set of intensity traces $I_q(\Delta E)$ for a fixed scattering angle (Trebbia and Colliex(3)).

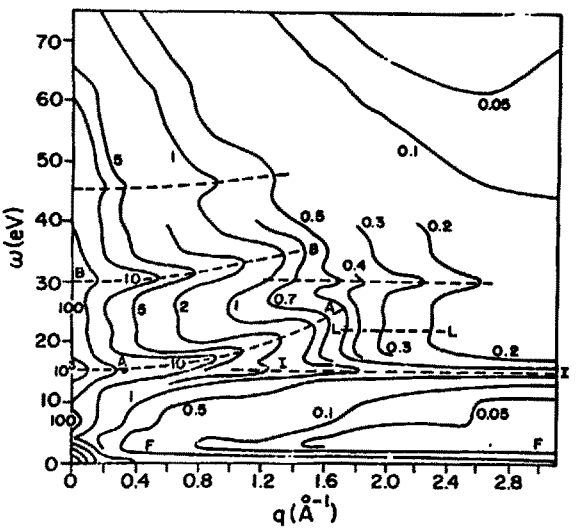

Fig. 1 : Intensity contour map $I(q,\Delta E)$ for a 500 Å thick aluminium sample with primary electrons of 75 kV (from Batson (2)).

In this simple description in terms of elastic and inelastic collisions, one omits the very important contribution of multiple scattering, that is the probability for an incident electron to be scattered m times elastically (without change in energy) and n times inelastically (with changes in energy ΔE_1, ΔE_2 ... ΔE_n) so that the total change in energy is $\Delta E = \sum_i \Delta E_i$.

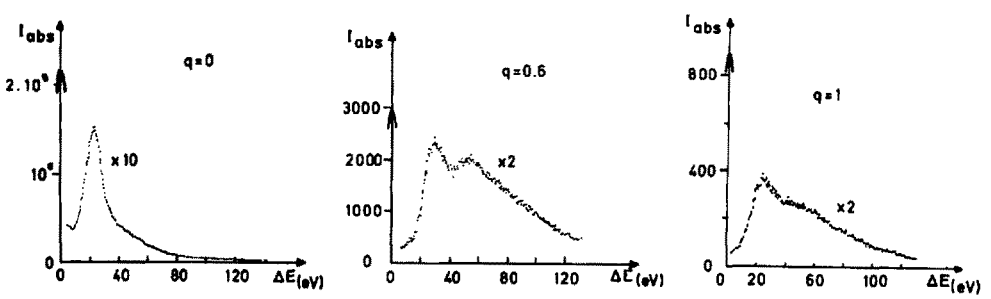

Fig.2 : Energy distribution of 50 kV electrons transmitted through a 250 Å thick carbon film for various momentum transfers (from Trebbia and Colliex (3)). q-values are given in $\mathring{A}^{-1}$.

Misell (4) has proposed a classification of these various processes within a probabilistic approach using a statistical Poisson law for multiple events. A single process is characterized by the distribution of the scattered electrons as function of the angle of scattering and the transferred energy, that is for a single elastic collision :

$$I^1_{el}(\theta,\Delta E) = I^1_{el}(\theta).\delta(\Delta E)$$

and for a single inelastic collision :

$$I^1_{in}(\theta,\Delta E) = F^1_{in}(\theta).G^1_{in}(\Delta E)$$

if one assumes that it is possible to separate the behaviour in energy and in angle (the validity of this hypothesis will be discussed later on). By performing some simple integrations, one finds that the total probability for single elastic scattering is : $I^1_{el} = \int_\theta \int_{\Delta E} I^1_{el}(\theta,\Delta E)d\theta d\Delta E = \frac{t}{\Lambda_e}$ where t is the specimen thickness and Λ_e the elastic mean free path. Similarly for single inelastic scattering : $I^1_{el} = \int_\theta \int_{\Delta E} I^1_{in}(\theta,\Delta E)d\theta d\Delta E = \frac{t}{\Lambda_i}$ where Λ_i is the inelastic mean free path. For 100 kV primary electrons orders of magnitude of mean free paths are :

Å		Carbon	Aluminium	Gold
Elastic	Λ_e	1300	700	60
Inelastic	Λ_i	600	500	400
Z		6	13	79

These values have been shown to obey an approximate law : $\frac{\Lambda_e}{\Lambda_i} \simeq \frac{20}{Z}$; it results that for moderate specimen thicknesses the probability of single scattering becomes greater than 1. Multiple events must be taken into account and the above expressions are to be modified as follows :

-) multiple elastic scattering :

Angular distribution : $I^m_{el}(\theta) = I^{m-1}_{el}(\theta) * I^1_{el}(\theta)$

$$I_{el}(\theta) = e^{-t/\Lambda_e} \sum_{m=1}^{\infty} \left(\frac{t}{\Lambda_e}\right)^m . \frac{I^m_{el}(\theta)}{m\,!}$$

Total probability : $I_{el} = \int_\theta I_{el}(\theta)d\theta = 1 - e^{-t/\Lambda_e}$

-) multiple inelastic scattering :

$$I^n_{in}(\theta,\Delta E) = I^{n-1}_{in}(\theta,\Delta E) * I^1_{in}(\theta,\Delta E) = F^n_{in}(\theta).G^n_{in}(\Delta E)$$

$$I_{in}(\theta,\Delta E) = e^{-t/\Lambda_i} \sum_{n=1}^{\infty} \left(\frac{t}{\Lambda_i}\right)^n \frac{I^n_{in}(\theta,\Delta E)}{n\,!} = F_{in}(\theta).G_{in}(\Delta E)$$

Total probability :

$$I_{in} = \int_{\theta} \int_{\Delta E} F_{in}(\theta) G_{in}(\Delta E) d\theta d\Delta E = 1 - e^{-t/\Lambda_i}$$

-) combined elastic-inelastic scattering :

The probability of m elastic interactions and n inelastic ones is given by the Poisson distribution :

$$P_{mn} = \frac{e^{-t/\Lambda_e}}{m\,!}\left(\frac{t}{\Lambda_e}\right)^m \cdot \frac{e^{-t/\Lambda_i}}{n\,!}\left(\frac{t}{\Lambda_i}\right)^n$$

Three main contributions can then be defined, the unscattered one corresponding to m = 0 and n = 0, the elastic one with m varying from 1 to ∞ and n = 0, the inelastic one with n varying from 1 to ∞.

A summation rule can then be written :

$$1 = I_{un} + I_{el} + I_{in}$$

where :

*) $I_{un} = e^{-t/\Lambda_t}$ for m = 0 and n = 0

The total mean free path is defined by $1/\Lambda_t = 1/\Lambda_e + 1/\Lambda_i$

*) $I_{el} = e^{-t/\Lambda_i}\,(1 - e^{-t/\Lambda_e})$ for $\sum_{m=1}^{\infty}$ and n = 0

The correction term expresses the fact there is no inelastic scattering.

*) $I_{in} = (1 - e^{-t/\Lambda_i})$ for $\sum_{m=0}^{\infty}$ and $\sum_{n=1}^{\infty}$

In this classification the inelastic component contains the single inelastic process and all multiple elastic-inelastic processes with at least one inelastic collision. It can be refined when one considers more specifically the angular dependence :

$$I_{in}(\theta) = \sum_{n=1}^{\infty} \left(\frac{t}{\Lambda_i}\right)^n \frac{1}{n!}\left[e^{-t/\Lambda_i} \cdot F_{in}^n(\theta) + I_{el}(\theta) * F_{in}^n(\theta)\right]$$

In the bracket the first term represents the convolution of the true inelastic component with the unscattered one and the second term with the elastically scattered one. As it will be shown later that the angular spread of the inelastically scattered electrons is narrower than the elastic one, four main classes of scattered particles can be roughly distinguished within a graph in energy and momentum transfers (figure 3).

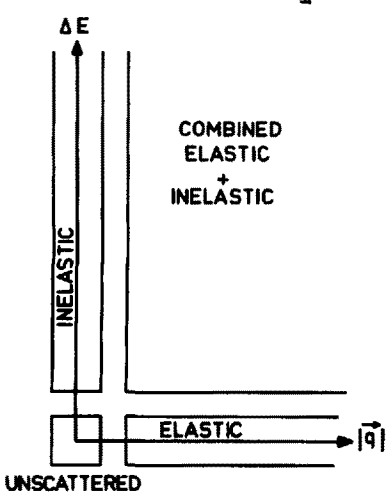

Fig.3 :

2. Single inelastic process.

2.1. Extraction of the single loss term :

As the elastic scattering is considered in Buxton's paper (this volume) the following part of this paper deals with the inelastic term, as defined in the previous section. This inelastic contribution is generally revealed as an energy loss spectrum, that is :

$$I_\alpha(\Delta E) = \int_{\theta=0}^{\alpha} I(\Delta E,\theta).2\pi\sin\theta d\theta$$

It represents the energy distribution of the electrons transmitted within an aperture of semi angle α. There does not yet exist a completely satisfactory deconvolution procedure to extract the single inelastic process from such an experimental spectrum and the generally used solutions implicitly assume a separation of the angular and energy dependence which is most satisfied when the angular acceptance α remains small.

In this small angle limit, various procedures have been developed to extract the single loss profile from an experimental one. Misell and Jones (5) have shown that the probability distribution of multiple scattering can be handled so that $I_1(\Delta E) = I_{exp}(\Delta E) - \frac{1}{2I_o}\left[I_{exp} * I_{exp}\right] + \frac{1}{3I_o^2}\left[I_{exp} * I_{exp} * I_{exp}\right] + \ldots$

where I_o denotes the unscattered peak intensity. To solve this equation it can be convenient to work in the Fourier spectrum. It has been used by Johnson and Spence (6), and this last author (7) has recently established how the Fourier coefficient $\tilde{I}_1(\tau)$ can be deduced from $\tilde{I}_{exp}(\tau)$ with the help of the simple algebraic relation :

$$\hat{I}_1(\tau) = \hat{M}(\tau).\ \mathrm{Log}\left[\frac{1}{I_o}\cdot\frac{\tilde{I}_{exp}(\tau)}{\tilde{G}_o(\tau)}\right]$$

This expression actually incorporates the instrumental impulse response with $\tilde{G}_o(\tau)$ and a gaussian filter $\hat{M}(\tau)$ to level out the noise which is introduced through these mathematical manipulations.

Another technique to solve these deconvolution equations is to calculate by iteration the spectrum for double, triple ... losses using step by step increments of the energy loss from the zero one. This procedure has been first described by Daniels et al. (8) in a general frame, then simplified by Wehenkel (9) and by ourselves (10) to be easily applied to the deconvolution of an energy loss spectrum between 0 and 150 eV.

Figure 4, concerning a 600 Å thick titanium foil, clearly displays the distribution of multiple events. The double plasmon appears as a satellite at about 35 eV on the onset of the peak which corresponds to the excitation of the 3p electrons. Similarly a faint structure on the experimental curve at 70 eV is due to double processes of type plasmon + 3p excitation. Both contributions are no longer visible on the deconvoluted curve.

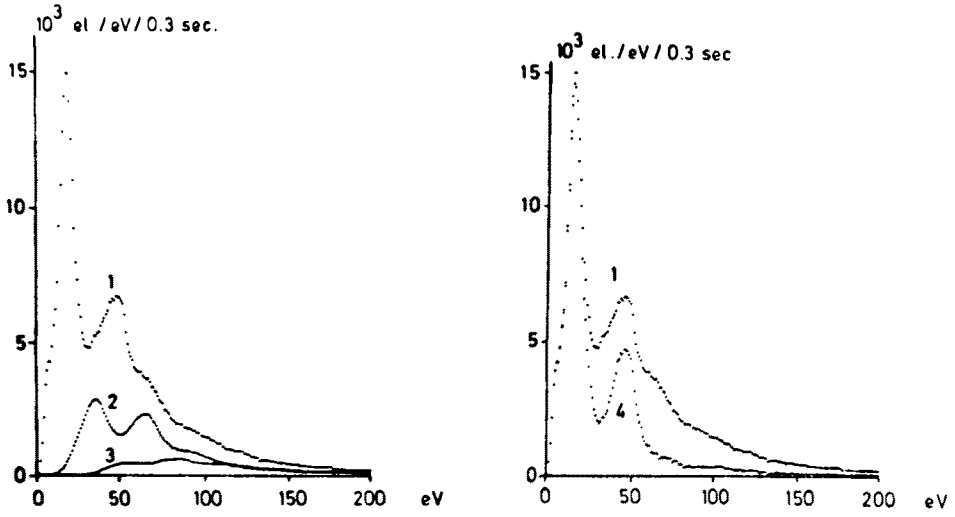

Fig.4 : Deconvolution of multiple energy losses by an iterative technique :
a) Curve 1 : experimental spectrum for a 600 Å titanium foil. Plasmon peak is at 17 eV and the maximum after 45 eV corresponds to the M_{23} edge.
Curve 2 : calculated double loss spectrum.
Curve 3 : calculated triple loss spectrum.
b) Curve 4 : result of the deconvolution, equal to Curve 1 - (2+3).

The validity of these data handling procedures has been checked for gold specimens of different thicknesses. From experimental spectra exhibiting quite noticeable differences it is possible to obtain a unique solution for the single loss profile.

2.2. Content of the single loss term :

It is beyond the scope of this paper to describe all the features of an energy loss spectrum. From two typical examples shown in figure 5, concerning a metal foil and a biological specimen, it is however possible to extract the general rules which govern the energy distribution of the electron excitation spectrum.

The first curve deals with a chromium specimen. Apart from the zero loss peak, it contains various structures corresponding to the excitation of the different electron populations in the target. From lower to higher energy losses they successively concern the conduction and the core electrons (atomic 3p at 50 eV and 2p at 575 eV). The first term appears as a peak at 24 eV generally labelled "plasmon" peak and the other ones as structures or edges superposed over a continuously decreasing background. Moreover, on this background, one detects stray

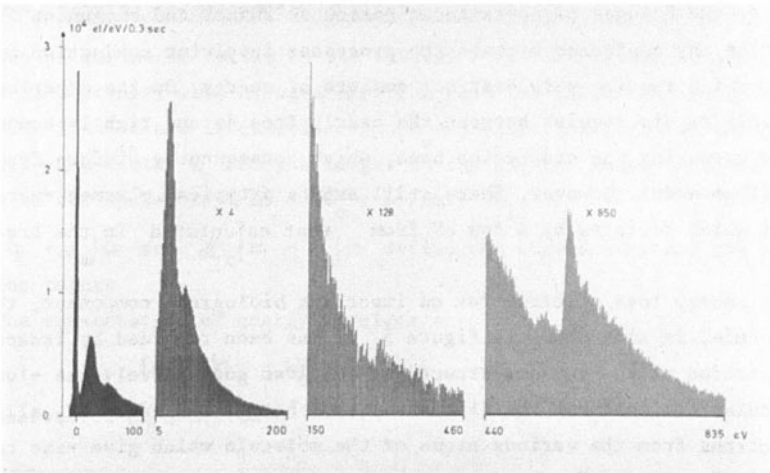

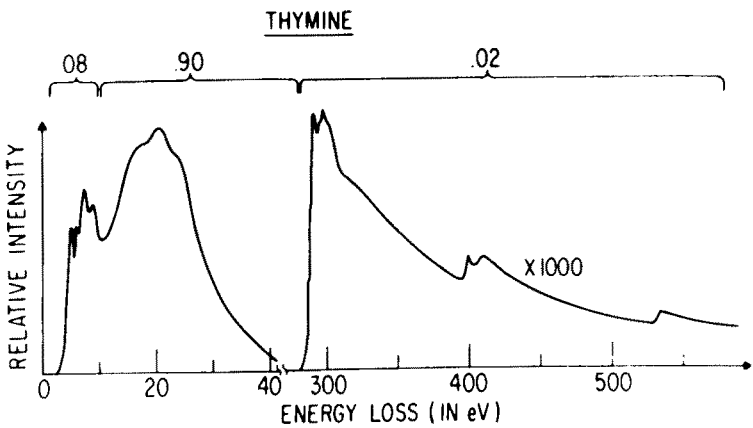

Figure 5 : a) Energy loss spectrum of 50 kV electrons transmitted through a 250 Å chromium foil. Because of the thinness of the specimen the multiple processes have not been subtracted. Semi angle of collection is 10 mrad. From left to right one sees the unscattered peak, the plasmon peak at 24 eV and the M_{23} edge at 50 eV. Contamination by carbon and by oxygen is revealed through their K signals respectively at 285 eV and 530 eV. They are followed by the chromium L_{23} edge at 580 eV. Notice the different intensity scales on the various curves.

b) Characteristic electron energy loss spectrum for a ≃ 500 Å thick film of the nucleic acid base thymine ($C_5N_2O_2H_6$) supported on a ≃ 20 Å thick carbon substrate. Primary energy of electrons is 25 keV. Structure due to both the valence shell and the inner shell excitations are shown. Above the spectrum, the relative fraction of the total inelastic scattering cross section is indicated for various energy regions (from Isaacson (11)).

signals due to the K edges of contaminant carbon at 285 eV and oxygen at 530 eV. There cannot be any confusion between the processes involving conduction and 3p and 2p electrons which require very distinct amounts of energy. On the other hand, it is not possible to distinguish between the nearly free 4s and tightly bound 3d electrons occupying the conduction band, which consequently differs from the standard jellium model. However, there still exists a typical plasmon energy, the value of which deviates by a few eV from that calculated in the free electron model.

An energy loss spectrum for an important biological component, the thymine molecule, is also shown in figure 5. It has been recorded by Isaacson (11). The interpretation of the various structures involves successively the electrons in the molecular orbitals for the fine structures between 5 and 10 eV, all the valence electrons from the various atoms of the molecule which give rise to a non characteristic "collective" term at about 25 eV which is visible for any carbonaceous material, and finally the atomic K edges for carbon, nitrogen and oxygen superposed on the background at respectively 285 eV, 405 eV and 545 eV. Such a spectrum is therefore interesting at two levels : the low energy fine structures, for instance the weak peaks at 4.8 eV and 7.4 eV, which characterize the molecular bonds with π orbitals, and the high energy core losses which can be used to determine the chemical composition of the molecule.

As a conclusion it is clear that an energy loss spectrum contains quite complete information concerning all the electron orbitals in the solid, whether they are rather localized in an atomic shell or delocalized through the conduction states of the solid.

3. Quantum mechanics formalism for an inelastic collision. Application to the study of the angular and energy distributions of the inelastic electrons

The analysis of the content of an energy loss spectrum shows that the solid behaves either as a collection of noninteracting atoms (for the characteristic core edges) or as a gas of interacting electrons (for the excitation of conduction electrons). It is consequently useful to treat the inelastic scattering of electrons either by an isolated atom, or at the other extreme, by an assembly of free electrons, a jellium, which consitutes the simplest approach for the description of the conduction electrons.

3.1. General formalism for an inelastic electron scattering :

For an inelastic collision the initial state is defined by the bracket $|\vec{k}_o 0\rangle$ that is a primary wave of wave vector $\vec{k}_o$ and the target in its fundamental state $|0\rangle$. The final state is described by $|\vec{k}_n n\rangle$, corresponding to an emerging electron with wave vector $\vec{k}_n$ and the target in the excited state $|n\rangle$. The total hamiltonian of the system is : $\mathcal{H} = \mathcal{H}_o + p^2/2m + \mathcal{H}_i$

where $\mathcal{H}_o|0\rangle = \varepsilon_o|0\rangle$ and $\mathcal{H}_o|n\rangle = \varepsilon_n|n\rangle$ define the eigenstates and the eigenvalues of the target.

The conservation of energy involves :

$$(\hbar^2/2m)(k_o^2 - k_n^2) = \varepsilon_n - \varepsilon_o$$

and the conservation of momentum :

$$\vec{q} = \vec{k}_n - \vec{k}_o$$

which gives, for the inelastic process depicted in the following sketch :

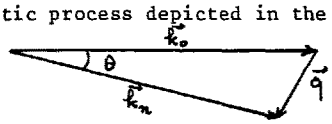

$$q^2 = (k_o - k_n)^2 + 4k_o k_n \sin^2\theta/2$$

The transition probability between the initial and final states is determined by the transition amplitude which, in the first Born approximation, reduces to :

$$T^{(B)}_{o\to n} = \langle \vec{k}_n n | \mathcal{H}_i | \vec{k}_o 0 \rangle$$

The interaction hamiltonian represents the Coulomb interaction between the incoming fast electrons and the electric charges in the solid target. Following the procedures which are developed in any quantum mechanics textbook, such as Messiah (1), one can calculate :

- the transition probability per unit time

$$W_{on} = \frac{2\pi}{\hbar} |T^{(B)}_{o\to n}|^2 \, \delta\left[\varepsilon_n - \varepsilon_o - \frac{\hbar^2}{2m}(k_o^2 - k_n^2)\right]$$

- the differential cross section between states 0 and n with ejection of the scattered particle of wave vector $\vec{k}_n$

$$\frac{d\sigma_{o\to n}}{d\Omega(\vec{k}_n)} = \left(\frac{m}{2\pi\hbar^2}\right)^2 \cdot \frac{k_n}{k_o} |T^{(B)}_{o\to n}|^2 \, \delta\left[\varepsilon_n - \varepsilon_o - \frac{\hbar^2}{2m}(k_o^2 - k_n^2)\right]$$

The last term can be shortened into $\delta(E_{tot})$ to express in simple terms the conservation of energy. The next step is to evaluate the matrix element for the transition in both models (isolated atom or jellium). As there exists strong analogies between both hamiltonians, one expects similar expressions. In the case of the single atom it has been established by Bethe (12) and a complete review is due to Inokuti (13). The jellium model has been thoroughly studied in a series of

papers by Pines and Nozières and a good survey can be found in the textbook by Pines (14).

3.2. Bethe theory for the inelastic scattering on a single atom :

Our purpose is to extract the useful formulae to evaluate the differential cross section in energy and in solid angle from which it is possible to deduce the angular and energy dependence for each type of inelastic process.

3.2.a. Cross section :

The initial and final wave functions are atomic ones, $|o\rangle$ describing the ground state one and $|n\rangle$ an excited one which can lie either in the discrete spectrum or in the continuum, in which case it is labelled as $|\varepsilon\rangle$ where ε represents the energy above the vacuum level.

$$\frac{d\sigma_{on}}{d\Omega(\vec{k}_n)} = \left(\frac{m}{2\pi\hbar^2}\right)^2 \cdot \frac{k_n}{k_o} \left|\langle n| \sum_{j=1}^{z} \frac{e^2}{|r-r_j|} e^{i\vec{q}.\vec{r}} |o\rangle\right|^2 .\delta(E_{tot})$$

can be transformed into :

$$\frac{d\sigma_{on}}{d\Omega(\vec{k}_n)} = \left(\frac{4\pi e^2}{q^2}\right)^2 .\left(\frac{m}{2\pi\hbar^2}\right)^2 .\frac{k_n}{k_o} .\left|\langle n| \sum_{j=1}^{z} e^{i\vec{q}.\vec{r}_j} |o\rangle\right|^2 .\delta(E_{tot})$$

Introducing the concept of generalized oscillator strength (GOS) defined as :

$$f_{on}(\vec{q}) = \frac{2m(\varepsilon_n-\varepsilon_o)}{\hbar^2q^2} \left|\langle n| \sum_{j=1}^{z} e^{i\vec{q}.\vec{r}_j} |o\rangle\right|^2$$

for transitions towards discrete states, and by its equivalent form :

$$\frac{df(\vec{q},\varepsilon)}{d\varepsilon} = \frac{2m(\varepsilon-\varepsilon_o)}{\hbar^2q^2} \left|\sum_{\Omega}\langle\varepsilon\Omega| \sum_{j=1}^{z} e^{i\vec{q}.\vec{r}_j} |o\rangle\right|^2$$

for transitions towards a final state in the continuum, defined by its energy ε above the vacuum level and by a set Ω of all other quantum numbers such as the angular momentum, the cross section can be expressed as :

$$\frac{d^2\sigma(\vec{q},\Delta E)}{d(\Delta E).d\Omega} = \frac{2me^4}{\hbar^2\Delta E} \cdot \frac{1}{q^2} \cdot \frac{df(\vec{q},\Delta E)}{d(\Delta E)}$$

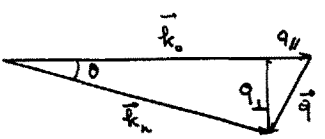

in the solid angle

$$d\Omega = \frac{2\pi}{k^2}.qdq$$

Using the simple relation extracted from the above scheme :

$$q^2 = q_{//}^2 + q_\perp^2 = k^2(\theta^2+\theta_E^2)$$

where $\theta_E = \Delta E/2E_o$ is a characteristic inelastic angle for an energy loss ΔE suffered by a primary electron of energy E_o :

$$\frac{d^2\sigma(\theta,\Delta E)}{d(\Delta E)d\Omega} = \frac{2e^4}{mv^2.\Delta E} \cdot \frac{1}{\theta^2+\theta_E^2} \cdot \frac{df(\vec{q},\Delta E)}{d(\Delta E)}$$

3.2.b. Angular dependence :

In the small angle limit, one can develop : $e^{i\vec{q}.\vec{r}_j} = 1 + i\vec{q}.\vec{r}_j + \ldots$ and the GOS can be extrapolated into its small q limit, that is the optical oscillator strength (OOS).

$$\frac{d^2\sigma(\theta,\Delta E)}{d(\Delta E)d\Omega} = \frac{4}{a_o^2 k^2} \cdot |x_{on}|^2 \cdot \frac{1}{\theta^2+\theta_E^2}$$

where the dipole matrix element is q-independent. As a consequence, the angular distribution of the scattered electrons behaves as $1/(\theta^2+\theta_E^2)$ at small angles, for any inelastic transition in an atomic collision. At large angle, deviations from this Lorentzian profile are introduced by the GOS. A three dimensional plot of $df(\vec{q},\Delta E)/d(\Delta E)$ in the coordinate system $(\vec{q},\Delta E)$ is known as the Bethe surface. As this surface embodies all the information concerning the inelastic scattering of charged particles by atoms, many experimental investigations as well as theoretical calculations of the GOS have been performed in atomic and plasma physics.

In the electron microscope it governs the behaviour of the electrons which are detected in the background or in an atomic core loss in the energy loss spectrum.

α) In the background case this atomic model can be used when most of the inelastic electrons have excited conduction electrons towards high energy states in the continuum. These electrons are reasonably considered as free because their binding energy is small when compared to the recoil energy which they get in the collision. Egerton (15), Leapman and Cosslett (16) have used this approach to interprete the angular distribution of the background electrons in an energy window located just below the K edge in carbon. The intensity is then peaked at an angle $\theta = (\Delta E/E_o)^{1/2}$; this maximum is known as the Bethe ridge, and corresponds in classical terms to close collisions with individual free electrons.

β) For core level excitations the GOS has recently been calculated for various inner shell electrons by using atomic wave functions $|n\ell\rangle$ and $|\varepsilon\ell'\rangle$ for the initial and final states (Leapman (17)). The GOS remains forward peaked at the edge, but at higher energy losses, it peaks at non zero momentum transfer corresponding to the Bethe ridge. Since the total angular distribution is weighted by the term $1/(\theta^2+\theta_E)$, it remains forward peaked but its width increases.

3.2.c. Energy dependence :

The energy loss spectrum, that is the energy dependent term, is estimated by the integral :

$$\frac{d\sigma_\alpha}{d(\Delta E)} = \int_{q_{min}}^{q_{max}} \frac{d^2\sigma}{d(\Delta E).d\Omega}\, d\Omega$$

where $q_{min} = k\,\theta_E$, and $q_{max} = k\alpha$ is set by the collection aperture. The energy differential cross section thus defined represents the gross shape of the energy distribution of a core loss signal. Profiles concerning the boron K edge, the magnesium L_{23} edge and the molybdenum M_{45} edge have been calculated by Rez and Leapman (18). Quite clear differences appear following the symmetry of the atomic orbitals which are involved in the transition.

3.3. Collective response for the jellium model :

3.3.a. Cross section :

The mathematical support is very similar to the one which has been used in the Bethe theory. Some minor changes are introduced in the terminology but they all express the close similarity between the matrix elements of the electron density (written as $\sum_{j=1}^{Z} e^{i\vec{q}.\vec{r}_j}$ in the atom and $\rho_{-\vec{q}} = \int \rho_{\vec{r}}\ e^{i\vec{q}.\vec{r}}\ d\vec{r}$ in the jellium), taken between the initial and final states of the transition. Starting from this fundamental analogy which has been established formally by Fano (19), the useful formulae are deduced by simple manipulations from those established in the Bethe theory. But instead of involving the GOS, they are generally expressed in terms of the energy loss function - Jm $1/\varepsilon(\vec{q},\omega)$, using the dielectric description of the electron gas introduced by Nozières and Pines. The cross section is then currently written as :

$$\frac{d^2\sigma(\vec{q},\Delta E)}{d(\Delta E).d\Omega} = \frac{1}{2\pi^2 E_o a_o} \cdot \frac{1}{\theta^2+\theta_E^2} \cdot \mathrm{Jm} - \frac{1}{\varepsilon(\vec{q},\omega)}$$

The energy loss function contains all the useful information concerning the response of the electron gas to the perturbation involved by the incident electron and is equivalent to the Bethe surface introduced in the atomic case.

3.3.b. Angular dependence

It is governed by the $(1/q^2)$.Jm $1/\varepsilon(\vec{q},\omega)$ factor. In the small angle scattering limit which corresponds to $|\vec{q}| \to 0$, one generally assumes that the momentum dependence of the energy loss function can be neglected so that :

$$\mathrm{Jm}\ \frac{1}{\varepsilon(\vec{q},\omega)} \to \mathrm{Jm}\ \frac{1}{\varepsilon(o,\omega)} = \mathrm{Jm}\ \frac{1}{\varepsilon(\omega)}$$

Similarly to the atomic case the angular distribution of the electrons which have been inlastically scattered by the conduction electron gas is mainly governed by the simple Lorentzian profile $1/(\theta^2+\theta_E^2)$ and this effect has been checked by Kunz (20).

However in this small angle approximation one misses the information concerning the electron excitation spectrum which is contained in the $\vec{q}$-dependence of the energy loss function. For instance the behaviour of the pole of this function $\omega_p(\vec{q})$ defines the dispersion law of the plasmon mode and, more generally, inelastic electron scattering experiments constitute one of the few efficient tools to investigate non vertical transitions for the electron gas of the solid. Raether (21) has recently reviewed some of the problems of interest which are presently investigated in this field : the anisotropy of the dispersion curves reflecting band structure features, the behaviour of the plasmon mode at large q values and its strong decay into electron hole pairs ... Such studies are still rather tricky because of the great difficulties encountered when one wants to extract a single inelastic profile from a large number of multiple elastic-inelastic processes which constitute

the majority of the detected signal at large q. Though most of the experimental work has been devoted to the plasmon mode in aluminium there still remains uncertainties about its behaviour beyond the cut-off wave vector (Batson, Chen and Silcox (22)).

3.3.c. Energy dependence

In the small angle limit the energy loss function - Jm $1/\varepsilon(\omega)$ has been measured over an energy range extending from zero to a few tens of eV for many substances. For simple metals (alkali, Be, Mg, Al ...) and semiconductors such as Ge, Si ... it mainly consists of a single peak located at a frequency $\omega_p = (n_o e^2/m\varepsilon_o)^{1/2}$ which corresponds to the well known plasmon frequency. In such cases the jellium model is a reasonable approach and the dielectric coefficient can be calculated in the random phase approximation (RPA). For the plasmon energy $\hbar\omega_p$, the value of $-\mathrm{Jm}\ 1/\varepsilon(\omega_p)$ provides an estimate of the screening of the external electric perturbation by the dynamic collective response of the electron gas. When one fits the energy loss function with a Lorentzian profile centered at ω_p, such as

$$-\mathrm{Jm}\frac{1}{\varepsilon(\omega)} = \frac{\omega_p \cdot \omega_p^2 \cdot 1/\tau}{(\omega^2 - \omega_p^2)^2 + \omega^2/\tau^2}$$

the parameter τ is related to the energy half width of the plasmon peak $\Delta E_{1/2}$ by $\tau = \hbar/\Delta E_{1/2}$ and represents the lifetime of the plasmon. Values of about 10^{-16} s are quite typical.

For other materials such as compounds, insulators, transition and noble metals, the conduction electron gas differs from the jellium model because of the strong influence of more tightly bound electrons, such as the d-band ones. Standard procedures have then been established to extract the dielectric coefficients $\varepsilon_1(\omega)$ and $\varepsilon_2(\omega)$ from an energy loss measurement (see Daniels et al (8)).

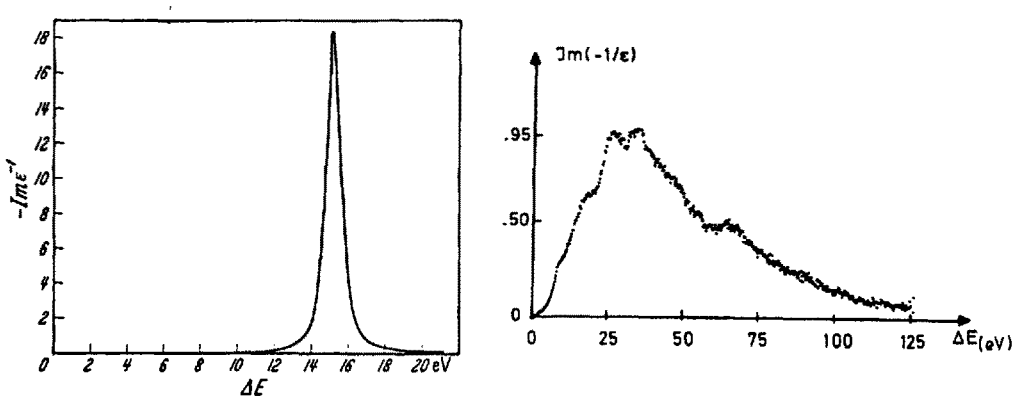

Figure 6 : Measured energy loss function in the limit $q \to 0$ for aluminium with a well defined plasmon peak, and for gold in which case the observed structures correspond to a complex mixture of interband and collective processes.

4. Microanalytical applications

When combined with the high resolution capabilities of the electron microscope, the use of electron energy loss spectroscopy (EELS) as an essential component for chemical microanalysis is a rapidly developing field, the limits of which remain to be firmly established. The general idea is to select a small volume of a sample and to detect useful signals in the energy loss spectrum of the transmitted electron beam. Although the project of obtaining elemental information from EELS was suggested by Hillier and Baker more than thirty years ago (23), it is only during these last few years that some obvious results could be obtained with this technique (Isaacson and Johnson (24), Colliex, Cosslett, Leapman and Trebbia (25), Colliex and Trebbia (10), Jouffrey et al (26)).

In the energy loss spectrum the chemical information is displayed over the whole distribution of inelastic electrons. One can use either the strong and poorly characteristic signals associated to the excitation of valence electrons (mainly plasmon lines) or the weak and truly characteristic core loss signals due to the ionization of atomic levels. Both types of information have actually been taken into account in various examples concerning material and biological problems. It is however generally admitted that the characteristic core level signals which provide an unambiguous tool for elemental recognition, offer greater promise for microanalytical purposes.

In a first operating procedure the energy loss spectrum is recorded for a selected specimen area, the size of which can be as small as 10 Å with a high resolution scanning transmission electron microscope (STEM). The detection of several excitation edges identifies the presence of the corresponding elements. Moreover quantitative analysis can be achieved by some simple handling of these signals. A core loss signal $S_c(\alpha,\Delta)$ is defined as the number of counts detected in a given conical solid angle of collection (half angle α) and corresponds to all characteristic events superposed on the background :

$$S_c(\alpha,\Delta) = \sum_{\Delta E=E_c}^{E_c+\Delta} (N_T(\Delta E) - N_B(\Delta E))$$

N_T and N_B represent the total and background number of counts in the channel located at ΔE in the loss spectrum.

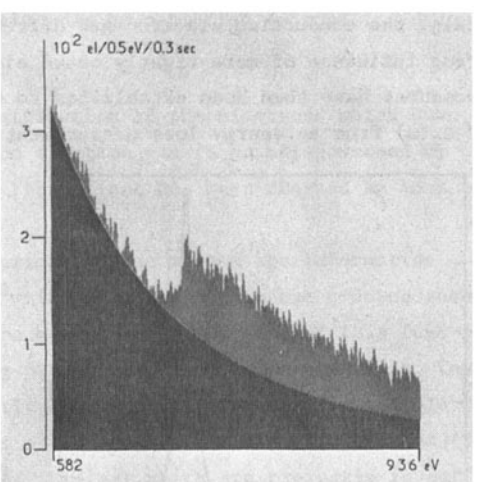

Fig.7 : Definition of the characteristic L_{23} signal for iron at 720 eV by extrapolation of the background following a power law.

Figure 7 shows a L_{23} edge for iron. The background is fitted with a power law $a\,\Delta E^{-r}$ by minimizing the standard deviation between the experimental and the model curves over a large energy domain, approximatively 150 eV broad, before the edge. One can then estimate the total number of atoms responsible for this signal, by using the formula proposed by Egerton (27) :

$$N = \frac{S_c(\alpha,\Delta)}{I_o(\alpha,\Delta)\sigma_c(\alpha,\Delta)}$$

where : - $\sigma_c(\alpha,\Delta)$ is the core loss cross section measured in a collection angle of half-width α and in an energy window Δ above the edge at E_c,

- $I_o(\alpha,\Delta)$ is the low lying energy loss contribution measured in the same conditions, that is involving the unscattered peak and the valence electron inelastic component from 0 to Δ.

In a binary alloy estimations of the concentration can be achieved by a ratio method with a rather good accuracy(Trebbia and Colliex (28)). The limits of the technique have been estimated as follows :

- the minimum detectable number of atoms is set by stability conditions at about one hundred atoms in present STEMS for a specimen which is not beam sensitive ; but radiation damage, which is particularly important for biological specimens,can raise this limit at about 10^6 to 10^8 atoms ;
- the low limit concentration depends on the extension of the analysed volume of material and it is evidently not possible to detect minority elements in a reduced assembly of atoms.

The resulting optimal domain of application for EELS is for the analysis of major elements in small volumes of typical size lying between 20 and 100 Å.

For many applications (for instance in the biological and mineralogical fields) the mapping of given elements over larger areas is most useful, and another working procedure, the filtered image energy selecting mode, provides an interesting solution. It consists of displaying an image of the sample with the electrons transmitted in a given energy window $\Delta E \pm \delta E$. By selecting plasmon images, El Hili (29) could thus characterize some well defined precipitates in aluminium based alloys. The systematic extension of this method however suffers severe limitations when one wants to use core loss signals. Besides the increased recording time associated with the weakness of the signal, the contrast in a filtered image us not only representative of the element associated with the edge, but also contains contributions from background variations due to thickness, density or crystal orientation changes. Jeanguillaume, Trebbia and Colliex (30) have discussed the limit of the method and suggested a few solutions to overcome this difficulty at the expense of more elaborate detection systems.

1. A. MESSIAH (1960), Mécanique quantique II, 687, Ed. Dunod

2. P.E. BATSON (1976), Ph.D Thesis, Cornell University

3. P. TREBBIA, C. COLLIEX (1978), Jap. J. Appl. Phys., Suppt. 17-2, 234

4. D.L. MISELL (1973), Advances in Electronics and Electron Physics, 32, 63

5. D.L. MISELL, A.F. JONES (1969), J. Phys. A, 3, 540

6. D.W. JOHNSON, J.C. SPENCE (1974), Proc. 8th Int. Conf. Electron. Microscopy, I, 386

7. J.C. SPENCE (1977), Proc. 35th EMSA Meeting, Boston, 234

8. J. DANIELS, C.V. FESTENBERG, H. RAETHER, K. ZEPPENFELD (1970) Springer Tracts in Modern Physics, 54, 77

9. C. WEHENKEL (1975), Ph.D Thesis, Université d'Orsay

10. C. COLLIEX, P. TREBBIA (1978), Electron Microscopy, State of the Art III, 268 Ed. J.M. Sturgess, Microscopical Society of Canada

11. M. ISAACSON (1975), Techniques in Electron Microscopy and Microprobe Analysis, 247, Ed. B. Siegel and D. Beaman, J. Wiley N.Y.

12. H. BETHE (1930), Ann. Physik, 5, 325

13. M. INOKUTI (1971), Rev. Mod.Physics, 43, 297

14. D. PINES (1963), Elementary excitations in solids, Ed. Benjamin N.Y.

15. R.F. EGERTON (1975), Phil. Mag.31, 199

16. R.D. LEAPMAN, V.E. COSSLETT (1977) Vacuum 26, 423

17. R.D. LEAPMAN (1979) Ultramicroscopy, 3, 413

18. P. REZ, R.D. LEAPMAN (1979) to be published

19. U. FANO (1956), Phys. Rev. 103, 1202

20. C. KUNZ (1961), Phys. Stat. Sol. 1, 441

21. H. RAETHER (1978), Jap. J. Appl. Phys., Suppt. 17-2, 227

22. P.E. BATSON, C.H. CHEN, J. SILCOX (1976) Phys.Rev.Letters, 57, 937

23. J. HILLIER, R.F. BAKER (1944), J. Appl. Phys. 15, 663

24. M. ISAACSON, D. JOHNSON (1975), Ultramicroscopy 1, 33

25. C. COLLIEX, V.E. COSSLETT, R.D. LEAPMAN, P. TREBBIA (1976), Ultramicroscopy 1, 301

26. B. JOUFFREY, Y. KIHN, J.P. PEREZ, J. SEVELY, G. ZANCHI (1978), Electron Microscopy, State of the Art III,292, Ed. J.M. Sturgess

27. R.F. EGERTON (1978), Ultramicroscopy 3, 243

28. P. TREBBIA, C. COLLIEX (1979), J. Microsc. Spectrosc.Electron, to be published.

29. A. EL HILI (1966), J. Microscopie 5, 669

30. C. JEANGUILLAUME, P. TREBBIA, C. COLLIEX (1978), Ultramicroscopy 3, 237